The Gemini-North Multiobject Spectrograph Integration, Test and Commissioning

Isobel M. Hook[a],J.R. Allington-Smith[b], S. Beard[c], D. Crampton[d], R. Davies[b], C.J. Dickson[c], A. Ebbers[d], M. Fletcher[d], I. Jørgensen[e], I. Jean[d], S. Juneau[d], R. Murowinski[d], R. Nolan[e], K. Laidlaw[c], B. Leckie[d], G.E. Marshall[c], T. Purkins[c], I. Richardson[e], S. Roberts[d], D. Simons[e], M. Smith[d], J. Stilburn[d], K. Szeto[d], C.J. Tierney[c], R. Wolff[f], R. Wooff[d].

[a] Department of Physics, University of Oxford, Nuclear & Astrophysics Laboratory, Keble Road, Oxford OX1 3RH, U.K.
[b]Department of Physics, Science Laboratories, University of Durham, South Road, Durham, DH1 3LE, U.K.
[c]UK Astronomy Technology Centre, Royal Observatory, Edinburgh, Blackford Hill, Edinburgh, EH9 3HJ, U.K.
[d]National Research Council of Canada, Herzberg Institute of Astrophysics, 5071 West Saanich Road, Victoria, BC, V9E 2E7, Canada
[e]Gemini Observatory, 670 N. A'ohoku Place, Hilo, Hawaii, 96720, USA
[f]National Optical Astronomy Observatories, 950 North Cherry Avenue, Tucson AZ 85719, U.S.A.

ABSTRACT

The first of two Gemini Multi Object Spectrographs (GMOS) has recently begun operation at the Gemini-North 8m telescope. In this presentation we give an overview of the instrument and describe the overall performance of GMOS-North both in the laboratory during integration, and at the telescope during commissioning. We describe the development process which led to meeting the demanding reliability and performance requirements on flexure, throughput and image quality. We then show examples of GMOS data and performance on the telescope in its imaging, long-slit and MOS modes. We also briefly highlight novel features in GMOS that are described in more detail in separate presentations, particularly the flexure compensation system and the on-instrument wavefront sensor. Finally we give an update of the current status of GMOS on Gemini-North and future plans.

Keywords: Instrumentation, Gemini, Imaging, Multi-Object, Spectroscopy

1. INTRODUCTION

In 1995, in planning for the first suite of scientific instruments which would operate on the new telescopes, Gemini chose to develop a pair of multiobject optical spectrographs, one for each telescope. The work for designing, developing, fabricating and testing these Gemini Multiobject Spectrographs (GMOSs) was assigned to a collaboration between the Particle Physics and Astronomy Research Council of the UK and the National Research Council of Canada, with the detector subsystem being provided by the Association of Universities for Research in Astronomy (US). The requirements for these spectrographs were chosen to take advantage of the superb seeing expected of the Gemini telescopes, while constrained by the relatively modest 7 arcmin field diameter which the telescopes would deliver. Further, as the only optical instrument on the northern telescope and the only Gemini instrument replicated at both sites, these GMOSs were intended to become the

Further author information: (Send correspondence to I.M.H)
I.M.H: E-mail: imh@astro.ox.ac.uk, Telephone:+44 1865 283106

optical workhorse instrument, and were assigned requirements which would lead to an instrument capable of performing a wide range of optical observations suited to many possible observing programs: direct imaging, longslit spectroscopy, multiobject spectroscopy and integral field spectroscopy.

Table 1: The primary requirements placed on the GMOS instruments

Wavelength Range	0.4 - 1.1 μm
Field	5.5 x 5.5 arcmin, limited to 7 arcmin diameter
Image Scale	0.072 arcsec per 13.5 μm pixel
Image Quality	Not degrade telescope I.Q. by more than 10%
Minimum slit width	0.2 arcsec
Spectral Resolution	R=5000 to R=500 with 0.5 arcsec slit
Velocity Stability	2km/s at R=5000
Optical Throughput	80% (not including filter or detector)
Integral Field Capability	Remotely deployable, 0.2 arcsec pixels with 50 arcsec^2 field (FOV as built = 52 arcsec^2)
Detector	6144×4608, 13.5 μm pixel CCD array

2. INSTRUMENT DESCRIPTION

The instrument uses an all-refractive optical design with f/16 collimator and f/4.9 camera, having platescales of 621 μm/arcsec and 187.5μm/arcsec respectively. A jukebox arrangement serves to load carbon fibre slitmasks or an integral field unit (IFU) into the 5.5 x 5.5 arcmin telescope focalplane which feeds the collimator. An on-instrument wavefront sensor (OIWFS) for tip, tilt and focus, as well as an atmospheric dispersion corrector are included in the instrument in front of the focalplane. At the collimated beam the user may select filters from the two filter wheels, each with 11 filter positions. The light path is folded at the collimated beam by either a mirror or one of three exchangeable gratings located in a grating exchange turret. The camera comes to a focus at the CCD array, located on a detector translation assembly (DTA) within the detector cryostat. The DTA[1] can displace the detector in focus, as well as in two directions orthogonal to focus to compensate in real time for instrument flexure while observing. Comprehensive overviews of the GMOS designs have been presented elsewhere.[2–4]

The OIWFS is used to facilitate precise acquisition of targets, provide accurate guiding and to improve image quality during exposures. The probe uses a small prism to divert the light of a relatively bright reference star. This light is analysed by a 2×2 Shack-Hartmann system running at, typically, 200Hz to deliver tip/tilt, focus and astigmatism correction signals to the telescope control systems. The probe pickoff arm patrols somewhat more than a quadrant of the GMOS focal plane, an approximately 15 arcmin^2 patrol field, by means of two rotary stages.[5]

Of the primary requirements listed in Table 1, those for the optical image quality and for spectral stability were decomposed into error budgets which served to guide the engineering and testing of subassemblies of the instrument. To develop the image quality budget, a starting point became the expected 10th percentile tilt-corrected seeing images expected at Mauna Kea: 0.274, 0.245 and 0.209 arcsec (50% EED) at 370, 500 and 1000 nm respectively. The Gemini telescopes are designed so as not to degrade these images by more than 15% and, in turn, the GMOS spectrographs are designed to degrade the best images delivered by the telescope by more than 10%. To achieve this, GMOS required an instrumental PSF of not more than 0.127, 0.113 and 0.097 arcsec (50% EED) at those same wavelengths.[7] The primary requirement for spectral stability, restated as a requirement for image motion of less than 3.125μm/hour (0.0167 arcsec/hour) at the camera focus, drove a

separate error budget which included terms for stiffness of mechanical structure, repeatability of mechanisms, and sensitivity to thermal effects.[6]

3. DEVELOPMENT PROGRAM

The GMOS instrument progressed through a series of design phases, culminating in its 1997 Critical Design Review with an accepted detailed design for the instrument. Following the design phase, sub-assemblies for each of the GMOSs were built by teams in Durham, Edinburgh and Victoria, and the CCD detector mosaic was integrated into the cryostat at Tucson. The sharing of effort among these four establishments required that individual modules be rigorously tested to ensure that their performance met the specifications at all orientations (gravity vectors) and anticipated operating temperatures (from room temperature to -5C). After subassembly testing, the modules, together with their control software, were brought together to be integrated and tested as a whole instrument at UKATC, Edinburgh.

The instrument integration and test phase followed a series of clear steps:

1. Instrument Integration, in which the sub-assemblies are coupled, control software integrated, and shown to remain functional,
2. Static Instrument Tests, in which instrument parameters which are not dependant upon gravity vector were characterized. These tests include overall optical alignment and performance, as well as instrument cold tests.
3. Dynamic Instrument Tests, in which the flexure control model was developed and the instrument was tested to be functional and meet performance requirements over a range of gravity vectors representing that experienced at the telescope.
4. Science Simulation Tests, in which the instrument was exercised in a manner which attempted to mimic observing sequences and conditions,
5. Acceptance Tests, in which the primary and derived requirements were demonstrated to be met and the instrument was demonstrated to conform to ICDs (interface control documents).

Following Acceptance Tests, GMOS was shipped to Hilo for integration and test with the Gemini control systems, transported to the summit, and began commissioning instrument modes. Following this, "System Verification" was carried out on the modes which would then become available to the Gemini communities. This phase involves an end-to-end test of the instrument and observing system, including observation preparation and data reduction.

4. INTEGRATION AND TEST RESULTS

The design requirements against which each test was made were guided by a suite of specifications and error budgets for optical tolerances, and for mechanical repeatability and stiffness. Here we discuss the results of some of these tests. Details of the optical and stability performance of GMOS may be found elsewhere in these proceedings.[6,7]

4.1. Mask and OIWFS Repeatability

The repeatability of the OIWFS probe arm's positioning was measured by monitoring the OIWFS reported tip-tilt values when staring at a fixed artificial star, and then moving probe away from and back to that focalplane position using a number of different directions of approach. Although the mechanical design strives to compensate for backlash by applying a constant loading torque on each of the two stages, best repeatability performance was found by using a software mode in which the target arm position was always approached from the same direction. When used in this way the OIWFS positioning repeatability was found to be better than 0.02arcsec at room temperature and better than 0.045arcsec equivalent on the sky at -5C. On-sky tests indicate that the required stability has also been achieved (see section 5.2).

The mask position in the focalplane is defined by spring loading the mask frame against three hard points. The repeatability was measured at −5C by moving a mask with a pinhole out and back in the beam, recording the pinhole image position at each trial. After 5 repetitions the RMS error in instrument X and Y, referred to the mask plane, are 0.3 and 0.8 μm (0.2 and 0.5 milliarcsec) respectively. The largest excursion is 1.7 μm (1.1 milliarcsec) in Y, which is well within the 25 μm (40 milliarcsec) spec: set to be equivalent to 1/5 of the minimum slitwidth.

4.2. Grating and Fold Mirror Repeatability

Each of GMOS's four grating cells has an integral gear sector to tip the grating in the optical fold direction, driven from a loosely fitting worm drive in the turret. To prevent the cell from moving within the range of the gear clearance under the influence of small perturbing forces, each cell is mounted on two bearings which are coaxial with the center of gravity of the cell, and which are specified to be overtight to provide additional bearing friction. The angle of tilt is determined by step counting the stepper motor which turns the worm drive. The tilt is datumed when necessary at the end of its travel with mechanical switches with a setting resolution of 6 pixels at the CCD (0.43 arcsec on the sky). During the test phase, we found that the best stability was achieved in all conditions by using a positioning sequence in which the cell was always brought to its resting position from the same direction, and then the worm drive was backed off a small amount to remove contact between the worm drive and gear sector, leaving the cell held in position by only the bearing friction.

There are three cases of operational interest in knowledge of the grating or mirror position: a) for comparison with data taken weeks or months ago, you may want to know how repeatable the grating is after remeasuring the datum point of the tilt drives, b) for comparison with daytime calibration or other data taken during the night, you might want to know how repeatable the tilt is after a period of a few hours and after a number of turret/grating movements have happened, and c) for its contribution to image quality and stability performance in a single observation, you will want to ensure its position remains sufficiently stable during a typical spectroscopic integration period of one hour. In case (c) the dominant effect is the differential flexure between the OIWFS and the slit, as described in more detail elsewhere in these proceedings.[6] The results, summarized in the Table 2, demonstrate that during a typical observing run the grating can be repositioned to better than 1/2 pixel (0.036 arcsec).

Table 2: Grating stability performance, measured during integration and Test in the lab at UKATC.

Case	RMS error at detector	RMS error (arcsec on sky)
After datuming grating tilt	$\pm$6pix = $\pm$81μm	$\pm$0.430
After a number of turret/grating moves	$<$ 0.44pix, $<$ 5.9μm	$<$ 0.032
During one hour of observation	$<$ 0.08pix, $<$ 1.1μm	$<$ 0.0056

4.3. Optical Results

GMOS was designed to exploit the excellent anticipated image quality and optimized for precise one- dimensional multiobject spectroscopy and two-dimensional integral field spectroscopy. The image quality requirement stated in 2 above, together with requirements for high throughput, minimal field distortion, insensitivity to thermal changes, good whole field image performance and good colour correction made the optics performance a natural centre of attention for much of the integration and test activity.

GMOS uses an all-refractive design with three lens groups for the collimator optics. The camera optical barrel also has three lens groups, and makes use of significant optical power at the window to the cryostat. The optical performance, described in more detail elsewhere in these proceedings,[7] delivers an image quality of better than 0.1 arcsec (50% EED) over the entire 400-1000 nm waveband, and a throughput of better than 70% over that same band (see Figure 1), while still satisfying the other constraints mentioned above.

4.4. CCD performance

GMOS uses three EEV (now Marconi) backside-illuminated CCDs, each of $2048 \times 4608 \times 13.5$ μm to give a 6144×4608 pixel focalplane. The imaging area falls on the central 4608×4608 area, with the longer dimension of the array placed in the dispersion direction to provide increased wavelength coverage for spectroscopy modes. The detector array is close packed, with about 0.5mm gap between detector imaging areas. Each CCD can be read out of either or both of its output amplifiers, with on-chip binning and fast skipping to multiple regions of interest possible. The detector controller operates the CCD readout at either a slow speed of 100 Kpix/s or fast speed of about 400Kpix/s with somewhat reduced read noise performance. Read noise for these detectors, measured in the integrated instrument on the telescope, is about 3 e- for each of the six amplifiers at the 100 Kpix/s speed. The sum of dark current and any light leaks seen with an open detector shutter inside the instrument enclosure is an average of below 2 e-/hr at its operating temperature of -120C and with the ambient light conditions similar to full moon. The CCDs are of normal epitaxial thickness, but have an antireflective coating which has been optimized for red performance, resulting in a quantum efficiency as seen in Figure 1.

The EEV CCDs in GMOS-North have significant fringing in the red. In imaging mode the fringe strength in the z'-filter is typically $\pm 2.5\%$ of the background, while in the i'-filter the fringing is $\pm 0.7\%$ of the background. In spectroscopy mode, where the effective spectral bandpass for each pixel is narrower, the fringing amplitude is larger, typically $\pm 12\%$ at 900nm. Example fringe frames in imaging mode obtained during commissioning may be found on the gemini web site, `www.gemini.edu/sciops/instruments/gmos/gmosIndex.html`

4.5. Thermal Results

Changes in temperature can adversely affect the instrument performance in a number of ways. Gradients in the predominantly steel structure of the instrument will cause optical components and assemblies to move with respect to each other; optics will require refocussing and will change optical prescription resulting in a plate scale change and image quality degradation; instrument enclosure air may stratify and cause seeing effects in the collimated beam; the ambient environment of regulated thermal systems such as the cryostat will change; and any number of mechanical effects may occur at interfaces of dissimilar metals due to the different thermal coefficient.

Records indicate that the nighttime temperature on the summit of Mauna Kea stays within -5C to +5C 95% of the time, and changes at a rate of less than 0.8C/hr. The GMOS instrument enclosure is thermally insulated so that the expected nighttime variations in the telescope enclosure temperature are further attenuated. Also, two fans mix the air within the instrument enclosure to prevent stratification and to help keep the structure thermally uniform. Our objective was to reduce the rate of temperature change seen within the instrument to a design value of 0.24C/hr, easing the requirements on thermal sensitivity on components within the instrument. At that rate of temperature change, plate scale changes without refocussing the instrument are reduced to 0.48 μm/hr at the edge of the field (as measured at the detector, where $1\mu m$ =5.4 milliarcsec on the sky). Image movement due to temperature slew, measured during cold tests to be 2.5 μm/C, is attenuated to 0.62 μm/hr. Both of these are acceptable values in the budget which partitions the total 3.125 μm/hr stability requirement. To date, due to the limited modes which have been commissioned, this level of stability has not been exercised with observations at Gemini. We're looking forward to commissioning the 2km/s mode of the instrument during the coming winter to find out how well these measures work in practice.

4.6. Instrument Flexure Results

Central to our strategy for meeting the 2 km/s velocity accuracy requirement within the allowed mass budget was to allow predictable elastic deformation of the structure as a function of gravity, and to use an open loop model in the instrument control system which adjusted the detector translation assembly to compensate for the expected amount of flexure-induced image motion. The development of this system is described in detail elsewhere in these proceedings.[6]

The effectiveness of the model was tested by measuring the movement of a mask pinhole image at the detector. With the flexure control system operating, the image movement in the dispersion direction, measured at the detector, was found to be 1.0 μm (or 5 milliarcsec) per hour in the average of many 'sweeps' covering

the accessible gravity vector space. The peak value measured was 2.5μm (13 milliarcsec) per hour. This was confirmed in a simulated tracking test which gave 0.96 μm (5 milliarcsec) per hour. A random pointing test was also done, simulating slews to new targets, which gave an RMS image movement of 3.0 μm (16 milliarcsec). All these results compare favourably with the 3.125 μm per hour required to meet the 2km/s velocity stability requirement.

The instrument flexure was re-measured once GMOS was mounted on Gemini-North. Some change in flexure performance is to be expected because of the Gemini Instrument Support Structure has different stiffness to that of the flexure rig used in the lab at UKATC. With the same sinusoidal flexure compensation model running as had been derived at UKATC, extensive tests were carried out during daytime by moving the telescope through a grid of of cassegrain rotator and elevation positions that cover the range used in normal observing. Mean flexure rates with the model running were measured to be 1.7 μm (9 milliarcsec) per hour in the dispersion direction and 0.6 μm (3 milliarcsec) per hour in the spatial direction, with peak measured values of 5.3 and 2.2 μm (28 and 12 milliarcsec) per hour respectively. This is somewhat worse than the values measured in the lab at UKATC, but sufficiently good for initial science use on the telescope. However in order to meet the 2km/s velocity stability goal (a mode yet to be commissioned) the flexure model should be updated on the telescope so that even the peak values are below the required 3.125μm/hr stability necessary for this mode.

4.7. Software Description and Performance

The GMOS software consists of the following components, built by a variety of different collaborators: A components controller (built by the HIA and UKATC) responsible for positioning the instrument's mechanisms, including the on-instrument wavefront sensor; A detector controller (built by the NOAO) responsible for controlling the shutter and detector temperature, as well as managing and reading out the science array; An instrument sequencer (built by the UKATC and Observatory Sciences Ltd.), responsible for coordinating the actions of the previous two components; An on-instrument wavefront sensor detector controller (built by the Gemini project and HIA).

The GMOS software follows the Gemini EPICS standard, using VME crates running VxWorks. Motor control is achieved through Oregon Microsystems (OMS) 8 and 44 cards controlled through an EPICS "device control record". The instrument assemblies are themselves coordinated using EPICS "assembly control records" which command the device control records and can be programmed with complex sequences of movements. This hierarchical design gives the software flexibility and allows it to be reused, and the EPICS control records developed for GMOS are now being used by other Gemini instruments. The software is controlled using engineering screens written using the EPICS "display manager" software. However, EPICS allows the software to be controlled and monitored from any client on the local area network using the EPICS "channel access" protocol. The instrument is now being controlled by the Gemini sequence executor, and will eventually be controlled from the Gemini Observatory Control system.

Because the GMOS software can be controlled from any channel access client, it is possible to make use of an automated test client. GMOS comes with a suite of test scripts, based on HIA's "dhsTestCmdr". All the test results are logged to a file which may be archived. This system allows comprehensive tests to be run on every software-readable instrument component in a few minutes, and it has been very powerful at revealing problems during instrument integration that may not have otherwise been noticed. During integration we adopted strict engineering practices and were careful to run the checkout scripts after any significant change to the hardware or software, or whenever the environment changed, for example during cold tests, flexure tests and before and after shipping. It is as a result of testing so rigorously with these scripts that the instrument has become very reliable.

5. ON-SKY INSTRUMENT CHARACTERISATION

Commissioning of the first GMOS on Gemini North took place in August 2001, beginning with daytime work (charaterisation of flexure etc) and followed by night-time tests. Below we summarise the main results.

5.1. Throughput

The throughput of GMOS in imaging mode was measured from observations of the standard star field[10] PG0231+051 on 2001 Aug 20 (UT). The data were reduced with the Gemini/GMOS IRAF package, using dome flatfields taken during the commissioning run.

Table 3: Preliminary throughput values - see text for explanation.

Filter	GMOS Predicted	Telescope	Atmosphere	GMOS Measured
g'	0.37	0.84	0.82	0.24
r'	0.61	0.83	0.88	0.49
i'	0.57	0.77	0.93	0.52
z'	0.19	0.82	0.91	0.16

Table 3, column 2 ("GMOS predicted") gives the predicted absolute throughput of GMOS based on the transmission of the main optics (i.e the collimator and camera lens groups), the filters and the QE of the CCD (see Figure 1). The GMOS Integration time calculator (ITC) was used to multiply these response functions with the telescope and atmosphere response functions, also summarised in Table 3, and thus derive expected counts for a given standard star magnitude (assuming spectral types, which were chosen based on the published broadband colours[10]). The telescope response is valid for the up-looking ISS port, through which these data were taken, and the atmospheric transmission corresponds to airmass=1.0. The ratio of the predicted and measured counts was then assumed to be equal to the ratio of the predicted and actual GMOS throughput, and the derived actual GMOS throughput is given in the last column of Table 3 ("GMOS measured").

It is likely that much of the discrepancy between the predicted and measured throughputs is in fact due to the primary and secondary mirror coatings. Subsequent cleaning of the primary mirror (May 2002) improved the reflectivity of the primary mirror by on average 6 percent, but still did not restore the reflectivity to that of newly coated aluminum. It should also be noted that the median extinction of Mauna Kea was assumed, and no independent measurement of the extinction for that night was made. These tests will be repeated.

5.2. OIWFS performance

The GMOS OIWFS utilizes the same CCDs and CCD controllers as most other Gemini wavefront sensors[11] but although a readnoise of < 4e- is realized in the laboratory, the best read noise achieved with GMOS on the telescope is ~ 7e-. The OIWFS has a 3 arcsec capture field and was designed to precisely maintain its location relative to the spectrograph input field. Tests indicate that this stability has been achieved (see below). In practice, the OIWFS has performed well on stars as faint as $R \sim 15$ (although not under bright moon conditions) when operating in a 2x2 binned mode and at 100 frames/s. Under these conditions, the sensor is delivering a signal to noise ratio of 20. In theory, it should be possible to use the OIWFS to guide on fainter stars. Experience with the SIS and HRCam guiding systems on the CFHT 3.6m telescope indicates that one should attain stable performance with a signal to noise ratio of 5 for tip/tilt only.[12] The optical and mechanical aspects of the GMOS OIWFS appear to be performing well but more sophisticated algorithms that automatically optimize its overall performance should be implemented to realize its full potential.

5.2.1. OIWFS flexure

The relative flexure between the OIWFS and the GMOS mask plane was measured by imaging a star through a large hole in a GMOS mask while guiding with the OIWFS. The mask also had several pinholes which allowed the mask-to-detector flexure to be monitored so that this could be subtracted from the star-to-detector flexure. The test ran for approximately 1.5hrs as the telescope crossed the meridian.

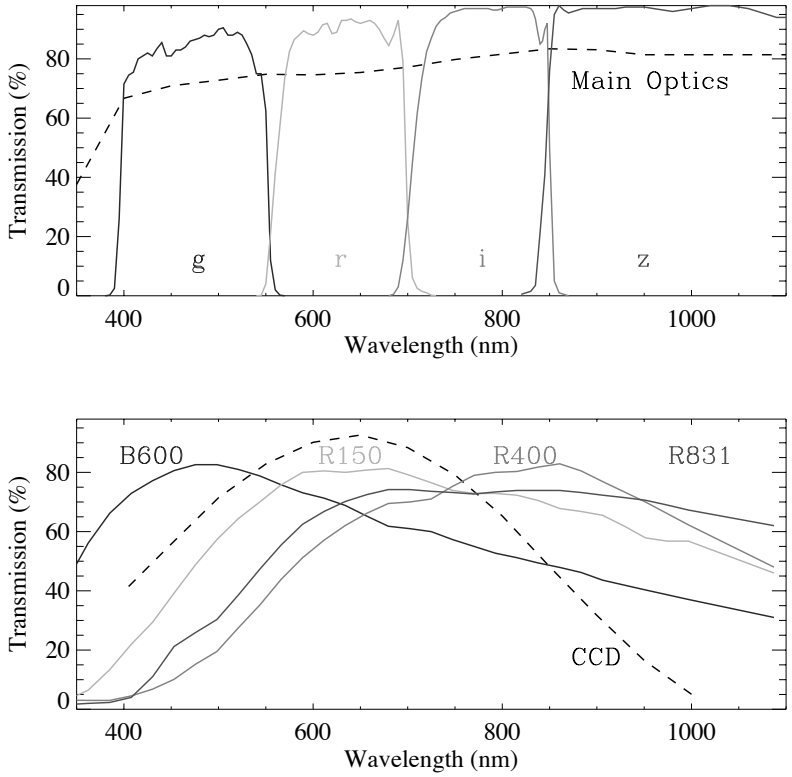

Figure 1. Optical response functions for the various elements currently in use in GMOS-N. The upper panel shows the transmission of the four science filters, g', r', i' and z', which are similar to the SDSS set,[9] and the main optics (i.e. the collimator and camera lens groups). The lower panel shows the average QE curve for the three EEV (now Marconi) chips and the response of the gratings, R150, R400, B600 and R831. The grating responses were measured in Littrow configuration by the manufacturers, and the wavelength scale in this figure has been shifted to account for the non-Littrow configuration in GMOS. Note that this is an approximation and that anomalies in the efficiency (sharp peaks and troughs) are difficult to predict when the geometry changes.

The test showed a small amount of OIWFS-to-mask flexure of 22 milliarcsec per hour in the dispersion direction and 3.6 milliarcsec per hour in the spatial direction(both measured at the science CCD). This compares favorably with results obtained from a similar test while guiding with one of the facility wavefront sensors, located much further away, which showed relative flexure of approx 100 milliarcsec per hour with respect to GMOS.

5.3. Maskmaker performance: uniformity of slits

Information on the choice of mask material, mask cutter and smoothness of slit edges has been published by Szeto et al.[8] The final chosen material is a 3-ply layup of carbon fibre in epoxy, supplied by Kinetics Composites Inc. of Oceanside, CA. The total thickness is 0.2mm and the fibre direction is set at 45 degrees from the edge of the mask, with the centre ply rotated 90 degrees from the outer plies. The slit smoothness has been measured from masks cut using the laser cutter at the Gemini Base Facility in Hilo. The 1 arcsec slits are generally smooth to better than 1% of the slitwidth.

6. SCIENTIFIC CHARACTERISATION AND VERIFICATION

During night-time commissioning of GMOS, data were taken in order to test the main modes of imaging, long-slit and multi-object spectroscopy (MOS). In many cases targets were chosen that had existing data from elsewhere for comparison. The commissioning data thus served the purpose of testing the acquisition procedure, data taking, data reduction and instrument performance for each mode. The majority of the GMOS commissioning data will be made public via the Gemini web pages, `http://www.gemini.edu/`. Here we describe some of the data obtained.

6.1. Deep imaging in the field of the $z = 4$ QSO PMN2314+0201[13]

Data obtained: This program involved deep imaging in the g, r and i bands. Dither sequences were defined which contained dither positions on a 10arcsec-spaced grid. The exposure times were 7×900s in the g band, 14×600s in r and 12×300s in i, taken on 2001 Aug23, Nov16 and Aug24 (UT) respectively. All were taken in dark conditions, using the detector binned 2x2 and in slow (100Kpix/s/channel) readout mode.

Data reduction: The reduction and combination of images was done using the Gemini/GMOS IRAF package. An attempt was made to use the images themselves to produce a "super-flat". Although this did a very good job of producing a flat final image (across all three chips), there were problems around bright objects because the dither steps were not large enough to cover them. Since the GMOS scripts do not currently have the functionality to mask objects from flats, twilight flats were used to flatfield the data. This gave better results around bright objects in the field, but some residual large scale gradients across the images, and steps between the three chips can still be seen, at approximately the 1% level. In addition, the g' and i' data show a large, circular patch of low-level light towards the top of the images. This was not present in the r' data. The effect has been seen very occasionally since then and its cause is not fully understood, but may be a reflection from the OIWFS.

Limiting magnitudes were derived from the coadded images using the zeropoints on the Gemini web pages. The values are given in Table 4 along with the image quality values derived from the combined images. These data provide a deep, multicolour dataset which can be used for many purposes.

Table 4: Summary of deep imaging data for the field of PMN2314+0201.

GMOS filter	Exp time (hr)	IQ	$m_{lim}(AB, 5\sigma)$
g	1.75	0.65″	27.5
r	2.33	0.68″	27.2
i	1.00	0.44″	26.3

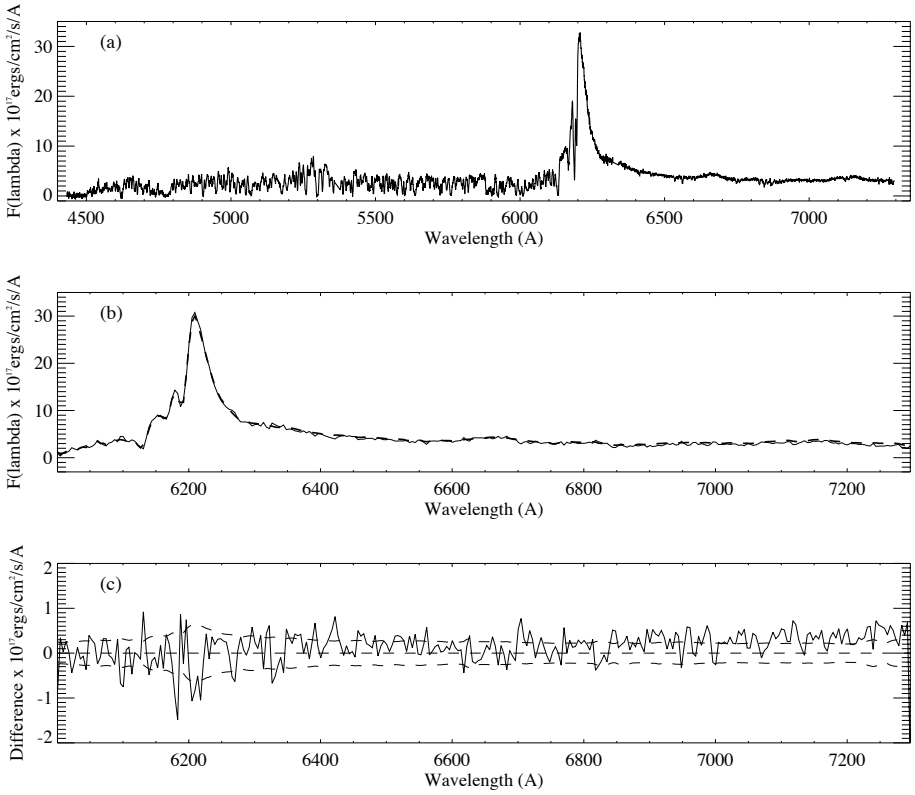

Figure 2. (a) Example of a GMOS longslit spectrum, a 900s exposure of the $z = 4.1$ QSO PMN2314+0201 (b) Comparison of the GMOS spectrum (dashed line) with a spectrum of the same object taken at the ESO 3.6m (solid line).[13] The GMOS spectrum has been smoothed to match the resolution of the ESO spectrum; (c) Difference between the two spectra (solid line) compared to the $\pm 1\sigma$ uncertainty (dashed line). Note the expanded flux scale. The slightly increased errors around the Ly-α line are probably caused by an imperfect match of resolution.

6.2. Longslit spectroscopic observations of PMN2314+0201

Data obtained A 900s observation of the $z = 4.11$ QSO PMN2314+0201 was taken on the night of 2001 Aug 15 (UT). The GMOS B600 grating was used, with a central wavelength setting of 600nm, and a 1.0arcsec slit, giving a wavelength coverage of 443-729nm and a spectral resolution of 0.6nm. Matching flats and arc comparison spectra were taken with the object data. Observations of the spectrophotometric standard Hiltner102 were also obtained with the same grating setting but a 5.0arcsec slit.

Data reduction and analysis The data were reduced using the spectroscopic tasks of the Gemini/GMOS IRAF package. Figure 2 shows the GMOS data compared to observations of the same object from the literature,[13] taken with the EFOSC spectrograph at the ESO 3.6m in Oct 1998. This is a 600s spectrum taken using the EFOSC R300 Grism (#5) and a 1.5arcsec slit, giving a spectral resolution of $\sim 1.9nm$. Despite the fact that neither spectrum was intended to be a spectrophotometric observation, their absolute flux levels agree to within the expected errors over most of the overlapping spectral range (see Figure 2).

6.3. MOS Observations of the cluster Abell 383

The cluster Abell 383 was observed on the nights of August 21, 26 and 27 2001 (UT) as a test of the MOS observing process, including pre-imaging, mask design, MOS field acquisition and observing. Figure 3 shows the pre-imaging observations, which were made up of 6 observations of 300s in the r band, dithered by 5 arcsec steps to cover the gaps between the chips. Matching g-band data were also obtained. The image quality in the r-band data was approx 0.65 arcsec FWHM.

From these data a mask was designed with 1.0 arcsec-wide, 9 arcsec-long slitlets placed on 22 objects in the field. In this case only one bank of slitlets was used, since the full width of the detector array is required for spectral coverage when using the B600 grating. Note that when a lower resolution grating is used, slits can be arranged in banks, so that up to about 400 slits can in principle be arranged on one mask. In addition four 2.0×2.0 arcsec boxes were included in the mask design for bright acquisition objects. The acquisition objects are used to align the mask to the sky, which can be done to an accuracy better than 0.1 arcsec.

MOS observations were taken through this mask on 26 and 27 August 2001. Five 1800s exposures were taken, using the B600 grating set to a central wavelength of 600nm (and no order-sorting filter). The MOS data shown in Figure 3 is the median of the three raw data frames from 27 August. The expanded section (approx 6 percent of the full frame) shows some galaxy spectra with emission lines. These give an example of the wealth of information contained in GMOS multi-object data.

7. CURRENT STATUS

The first GMOS has been in regular science use on Gemini-North since November 2001. At present the imaging, longslit, MOS and Integral Field Unit modes of GMOS-N have been commissioned. The IFU is the subject of a separate paper in these proceedings.[14] The Atmospheric Dispersion Corrector has yet to be fitted and commissioned (planned for early 2003), and hence the high velocity precision (2km/s) mode has not yet been commissioned.

A few changes have been made to GMOS since its arrival at Gemini-North. The cryostat has been fitted with a closed-cycle cooler to replace the liquid nitrogen cooling system. Also three new long-pass filters have been purchased and fitted (GG455, OG515, RG610). It is expected that more gratings will be purchased, although only three can be mounted in the instrument at any time. Finally, the Nod-Shuffle observing mode for accurate sky subtraction[15] is currently being implemented on GMOS-N. For details of the current status of GMOS and the complement of filters and gratings, see the the Gemini/GMOS web pages. `http://www.gemini.edu/sciops/instruments/gmos/gmosIndex.html`.

REFERENCES

1. P.R. Hastings, "Focus and translation mechanism for the Gemini Multi-Object Spectrograph (GMOS)", SPIE 2871, pp. 1216–1221, 1996.
2. Davies, R. L. et al. "GMOS: The GEMINI Multiple Object Spectrographs", SPIE 2871, pp. 1099 1106, 1996.
3. Murowinski, R. et al. "The GEMINI Multiobject Spectrographs", SPIE, 3355, 297, 1998
4. Crampton, D. et al. "Gemini Multiobject Spectrograph GMOS: integration and tests", SPIE 4008, p. 114-122, 2000.
5. Roberts, S., Fletcher, M., Leckie, B., Saddlemyer, L., Szeto, K., & Sebesta, 1997, SPIE, 3132, 184.
6. Murowinski, R. G. et al., Gemini-North Multi-object spectrograph stability performance, this conference, SPIE ref 4841-128
7. Murowinski, R. G. et al., Gemini-North Multi-object spectrograph optical performance, this conference, SPIE ref 4841-161
8. K. Szeto, J. Stilburn, T. Bond, S. Roberts, J. Sebesta, L. Saddlemyer, Fabrication of Narrow-Slit Masks for the Gemini Multi-Object Spectrograph, pp. 1262–1271, SPIE 2871, 1996
9. Fukugita, M., Ichikawa, T., Gunn, J. E., Doi, M., Shimasaku, K., Schneider, D. P, 1996, AJ, 111, 1748.
10. Landolt, A. U., 1992, AJ, 104, 340.
11. Leckie, B. and Hardy, T., "Gemini WFS CCDs and controllers", SPIE 3355, p. 529-538, 1998
12. LeFevre, O., Crampton, D., Felenbok, P., & Monnet, G., CFHT MOS/SIS Spectrograph, 1994, A&A, 282, 325.
13. Hook I. M., McMahon R.G., Shaver P. A., Snellen I. A .G., A&A 2002, in press
14. G. Murray et al. "Integral field spectroscopy with the GEMINI multiobject spectrographs", SPIE, this conference, ref 4841-195
15. K. Glazebrook, J. Bland-Hawthorn, 2001, PASP, 113, 197

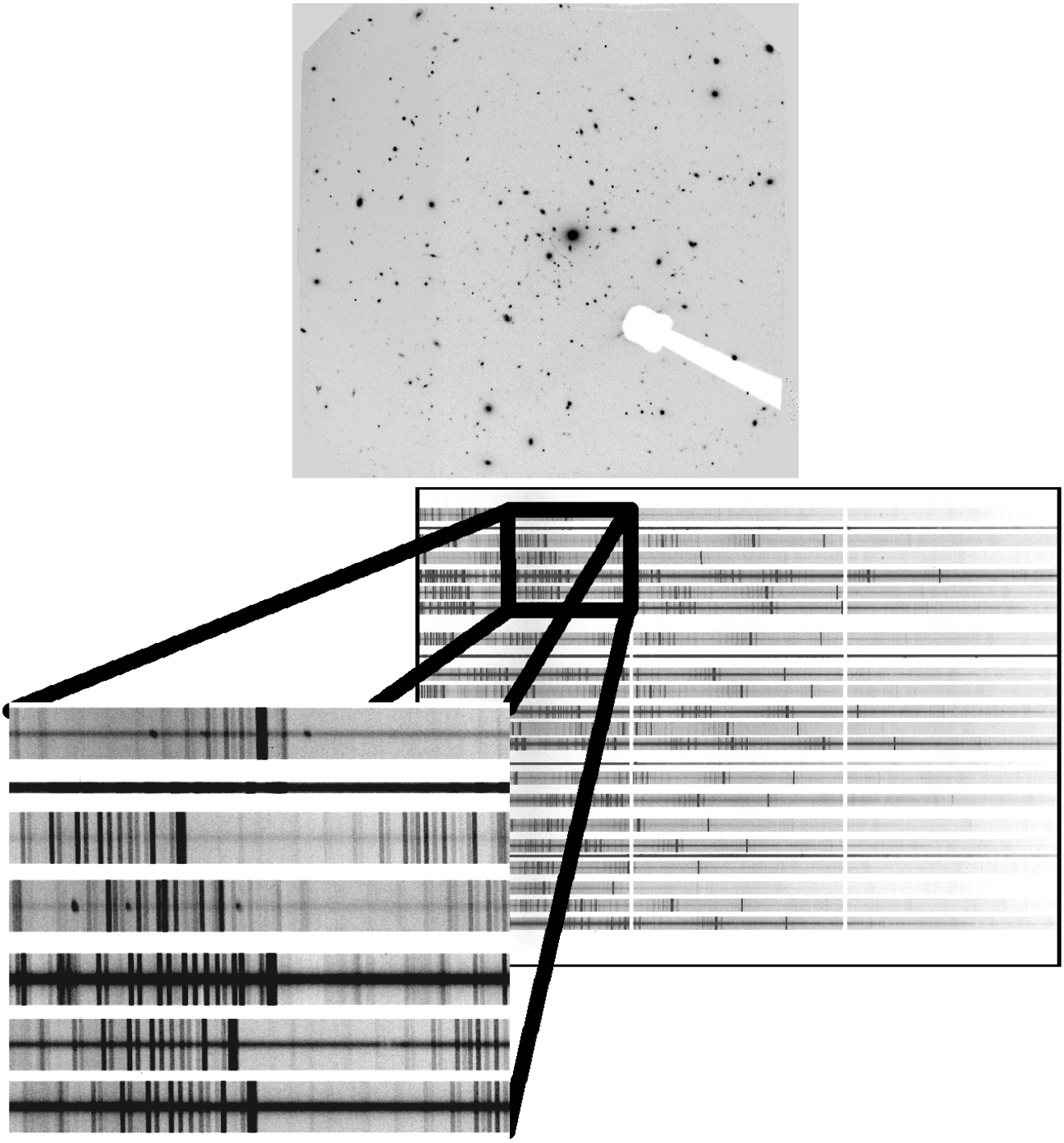

Figure 3. Upper frame: Full-frame ($5.5 arcmin \times 5.5 arcmin$) GMOS image of the cluster Abell 383, taken in the r-band. The shadow of the On-instrument wavefront sensor probe is visible in the lower right quadrant. Since this image is the combination of several dithered images, the gaps between the detectors have been covered. Central Panel: corresponding MOS data. Longer wavelengths are to the left. The gaps between the three CCD detectors are visible as vertical strips. In this example the mask had 22 slitlets for galaxies in the field plus 4 holes for acquisition objects to align the mask to the sky. Note that when a lower resolution grating or a filter is used, slits can be arranged in banks so that up to about 400 slits can in principle be arranged on one mask. Lower Panel: magnified region of the frame showing example galaxy spectra with emission lines.